Extended data and supplementary information for Complex viral evolution as an unintended consequence of social distancing

Simon Plakolb*, Patrick Mellacher

*Corresponding author. Email: simon.plakolb@ibv.uio.no

This PDF file includes:

Supplementary Text

Figures S1 to S12

Tables S1 to S5

Supplementary Text

Calculation of contact rate values

Our model is based on an influenza reference model (*1*) to describe the presence of low phylogenetic diversification in influenza strains. This reference model utilizes an agent-based approach where all individuals of the population are simulated individually. These agents are distributed uniformly within $M = 20$ geographically distinct patches. This method is computationally expensive, if the simulated number of people is large. We thus simplify this model to carry out the simulations in a more efficient way: We assume homogeneous mixing within each geographical patch. This allows us to model the spread of the virus using the well-known SIR equations. However, since we are interested in tracking viral evolution, we also want to explicitly model a potentially large number of virus variants. To do so, we use an agent-based approach where we model each variant as an agent (instead of each person).

To account for the differences in the modeling approach, we have to carefully adjust the contact rates in our model. The influenza reference model differentiates between local transmission with a contact rate determined by β_L, mixing within a patch with β_W and contact between patches with β_B. The reported basic reproduction number for transmission within local groups is $R_0 = 5$. Within a geographical patch, transmission is less likely with $R_0 = 0.4$ and transmission in between patches is given with $R_0 = 0.02$.

We find our values for $\beta_{W,0}$ and the homophily parameter h using equations S1 and S2 (*32*):

$$\beta_{W,0}(h + \frac{1-h}{M}) = \frac{5.4}{\gamma_0^{-1} + \mu_0^{-1}} \tag{S1}$$

$$\beta_{W,0}\frac{1-h}{M} = \frac{0.02}{\gamma_0^{-1} + \mu_0^{-1}} \tag{S2}$$

The resulting parameter values are listed in Table 1 of the manuscript. To gain an intuition for these equations, one can rewrite their left-hand side (LHS) with $M = 20$. Equation S1's LHS then reads as $\frac{1}{20}\beta_{W,0}(19h + 1)$. It can be understood as the local transmission component. In a completely homophilic $h = 1$ scenario $\beta_{W,0}$ equals the right-hand side (RHS) of S1. For equation S2 the LHS

can be rewritten as $\frac{1}{20}\beta_{W,0}(1-h)$. In a scenario with homogenous mixing between all patches ($h = 0$), $\beta_{W,0}$ corresponds to the RHS of S2. Intuitively, the homophily parameter h regulates the balance between both extremes.

Reproduction scenarios

Despite our methodological changes, our model can reproduce the results of the influenza reference model [see (*1*)]. As listed above [see Methods in Section 3], all but one parameter are set to the values of the reference model. Our method necessitates some changes to the immunity model. Therefore, as described in our methods section, the cross-immunity's minimal effect θ_0 was reduced.

Fig. S1 shows our reproduction of the influenza reference model's results in two key scenarios that follow the methodology of its source (*1*). A setting with low mutability and *only* cross-immunity is compared to a scenario paring high mutability with an additional non-specific immunity. Both scenarios were evaluated with each using 50 simulation runs over 30 virtual years.

Pane **A** of Fig. S1 shows the weekly incidence in the first geographical patch. Much like in the influenza reference model's associated report, the scenario excluding the non-specific immunity peaks between $10,000$ and $15,000$ inhabitants in the first 15 years. The incidence for the scenario including the non-specific immunity is lower. In the second half of the simulation, it peaks around $3,000$ inhabitants, again resembling the reference result (*1*). The reference's units are reported to be per $100,000$ inhabitants (*1*). We find that this may be an error in these units, as the percentage of infected inhabitants appears unrealistic. In any case, our model produces a similar difference between both scenarios. More importantly, our observations for pairwise diversity match those reported for the influenza reference model (*1*).

In pane **B** of Fig. S1 a lack of non-specific immunity proves to lead to rapid diversification. Meanwhile, the added non-specific immunity component limits diversification drastically, despite a tenfold increase in mutability. In both cases, the range of the pairwise diversity closely resembles that reported for the influenza reference model (*1*).

Equations of the reproduction model

Our model includes a pre-symptomatic phase and asymptomatic cases. In contrast, the influenza reference model (*1*) uses a single mode of symptomatic infection. Furthermore, it does not consider the possibility of a lethal infection outcome. Therefore, some equations listed in our manuscript's methods section can be simplified to reproduce this model.

The population that is cross-immune to variant i and currently within the compartments specific to any variant can be calculated without the $P_{p,i}$ and $A_{p,i}$ compartments:

$$C_{p,i,I+F} = \sum_j (E_{p,i} + I_{p,i} + F_{p,i})(1 - f(d_{i,j}))\frac{C_{p,i}}{N_p} \tag{S3}$$

We want to reiterate the intuition for this expression. For a variant i, the sum of the cross-immune population needs to be scaled to reflect a good estimate. We assume a reasonably good mixing within all compartments. Then, the fraction of the cross-immune individuals within the total population $\frac{C_{p,i}}{N_p}$ can be used for the variant-specific cross-immunity compartments. However, the likelihood of a cross-infection is inversely correlated to the cross-immunity. Thus, an additional scaling by $1 - f(d_{i,j})$ is necessary.

Due to the reduction of infection compartments the normalized contagious population $I_{tot,p,i}$ simplifies to a mere fraction of symptomatic individuals within the population:

$$I_{tot,p,i} = \frac{I_{p,i}}{N_p} \tag{S4}$$

Since there are no more pre-symptomatic and asymptomatic cases, the exposed population in $E_{p,i}$ flows directly into $I_{p,i}$:

$$\dot{I}_{p,i} = \alpha_i E_{p,i} - \gamma_i I_{p,i} - \frac{I_{p,i}}{L} \tag{S5}$$

Likewise, the absence of lethal consequences simplifies the compartment outflow of $\dot{I}_{p,i}$. As in all compartments, the life expectancy L governs the rate of natural death. Besides the natural deaths, only γ_i regulates the outflow by determining the mean infection duration. Consequently, the net recovery rate reduces to only the net flux out of the infected compartment:

$$\dot{R'}_{p,i} = \gamma_i I_{p,i} \tag{S6}$$

For the scenario excluding the non-specific immunity the model can be further simplified. In this scenario the non-specific immunity compartment F_p and the associated, variant-specific state variable $F_{p,i}$ can be excluded from the model. The component for the variant-specific susceptible population $S_{p,i}$ can then be rewritten as:

$$S_{p,i} = S_p - C_{p,i} + C_{p,i,I} \tag{S7}$$

It uses the cross-immune population currently infected by other variants $C_{p,i,I}$. It is an alternative to $C_{p,i,I+F}$ that excludes the non-specific immunity compartment F_p:

$$C_{p,i,I} = \sum_j (E_{p,i} + I_{p,i})(1 - f(d_{i,j}))\frac{C_{p,i}}{N_p} \tag{S8}$$

Excluding F_p also changes the flux of recovered individuals. The recovered population flows directly into the susceptible compartment, for which the derivative changes to:

$$\dot{S}_p = \frac{N_p}{L} + \left(sum_i \gamma_i I_{p,i} - b_{p,i} S_{p,i}\right) - \frac{S_p}{L} \tag{S9}$$

Without the non-specific immunity, recovered individuals directly contribute to the cross-immunity. Therefore, the cross-immunity derivative is now given by:

$$\dot{C}_{p,i} = \sum_j f(d_{i,j})\gamma_j I_{p,j} - \frac{C_{p,i}}{L} \tag{S10}$$

The influenza reference model (*1*) deals with the evolution of a pathogen with widespread antigenic adaption in the population. Thus, simulations start "near the single-strain equilibrium" (*1*). To reproduce this, we disable all mutations in the first 100 simulated years to arrive at the (dynamic) single-strain equilibrium. Afterwards, we enable mutations. As in the influenza reference model, in our reproduction model the epidemiological parameters are not affected by the mutation but constant. The parameters used in the reproduction model are listed in Table S2.

Our model under equilibration

The substitution of the host-agents with ODEs is not the only difference the between the influenza reference model (*1*) and ours. Due to the focus on a different, and novel, pathogen our method introduces new compartments and the mutation of epidemiological parameters. In addition, the scenarios in our study start before the single-strain equilibrium establishes itself. Arguably, there is a large gap between the reproduction scenarios and our main study. To bridge this gap, we additionally investigate a scenario of our novel model starting close to the single-strain equilibrium. This scenario uses the main study's base scenario parameters. There are no pharmaceutical or non-pharmaceutical interventions. Note that these parameters do not differ drastically from the reproduction model.

The additional compartments of the epidemiological model exhibit only a minor impact on the population dynamics. The most notable difference to the reproduction scenarios appears to be the quicker establishment of a dynamic equilibrium. This is likely the effect of the extended latent period.

Our scenario includes a non-specific immunity component. Consequently, the pairwise diversity is reduced. For the influenza reference model, one can show that functional constraints on the viral evolution do not significantly impact the results (see Supplementary Material of (*1*)). Using our model, which decouples the stylized RNA mutation from the evolution of epidemiological parameters, we find that only after the first $\sim$ 15 years the parameter mutation starts to impact the pairwise diversity. We, therefore, conclude that the long term effects of the interventions in our model should be investigated at the 15 year mark.

Sensitivity Analysis

To improve the insight into our model's dynamics, we perform a sensitivity analysis beyond the scenarios shown in Fig. 2. Each parameter combination is evaluated at least 50 times with varying pseudo-random number generator seeding. The sensitivity analysis focuses on the state after 2 and 4 simulated years. Some parameter combinations, however, cover a time span of 15 or 30 years to investigate the long term dynamics.

Intervention model analysis and long term results

Our scenarios cover a large range of the two main intervention model parameters. In our main results figure, we show the correlation of various metrics with the peak size of the non-specific immunity population for a varying intervention effect β_b. The same analysis can be done for the intervention threshold τ_b. Fig. S3 shows these correlation plots using a fixed intervention effect β_b of 90 ‰. Most R^2 values are lower compared to the main results pane **D** in our manuscript. Only the pairwise diversity metric appears to react stronger when varying τ_b with a fixed β_b.

Due to a lack of space in our main results figure, only two entropy metrics show the results after 15 years. In Fig. S3 we show the state of other key metrics in our study throughout the 15 th year. We find that the pairwise diversity reaches a similar equilibrium in all scenarios. The size of the population with non-specific immunity is, however, much larger in the scenario without interventions. This is reflected in the entropy metrics which are lower in these scenarios. Contrary to our intuition, without the interventions the linearity is lower than in any of the intervention scenarios on average, even though the variance is higher. This could be a latent effect of the delayed second infection wave.

In Fig. S4, we take a look at some exemplary phylogenetic trees. All example trees show the 500 variants with the largest recovered or infected population and their ancestry. The blue trees show the phylogeny after 15 years without the interventions (**A**) and for a scenario of category C (**B**). Significantly more diversification events are visible in the blue tree shown in **B**. This explains the difference in the Λ values. Table S5 lists the associated metrics for the aforementioned trees. It is easy to see, that the entropy measures and the tree linearity focus on the entire structure of a phylogenetic tree. In contrast, pairwise diversity (PD) quantifies the temporary state. This is especially noticeable in the values for the black trees which show the state after 30 years. An additional example of a scenario with vaccinations is shown in pane **C**. At its right end this tree shows more concurrently circulating variants the other examples in **A** and **B**. It exhibits a pairwise diversity of 7.14. In comparison, this is significantly higher. This difference is not reflected in the rest of our used metrics. This points to the complementary nature of these metrics and to the benefit of their use in unison.

Our simulations end after a period of 30 years. The effects of the parameter mutation on the

evolutionary patterns already explored in Fig. S2 can be revisited here. Fig. S4 **D** suggests that the scenario lacking interventions may be more resilient to the effect of the parameter mutation. In contrast to the other scenarios, its pairwise diversity is less elevated. This can also be seen in the example trees (**A** - **C**) that show the phylogeny after 30 years.

Analysis of epidemiological and mutational characteristics

The main driver for the evolutionary dynamics in our focus is the intervention model. However, there is a complex interplay between it and the other model parameters. We extend our analysis to cover the parameters that had to be changed from the source values or were newly introduced. First, we focus on the state after 2 years, *i.e.*, the state immediately preceding the end of the interventions. The model component parametrized based on the influenza reference model (*1*) differs in two parameters from the source. The contact rate β_W uses a homogeneous mixing based estimate. The minimal effect of the cross-immunity θ_0 was adapted to the differences in the cross-immunity model.

The scenario category C covers the scenarios with the strongest effect of the non-pharmaceutical interventions on our results. Thus, we model the interventions for this category with a threshold of $\tau_b = 10^{-6}$ and an intervention effect β_b of 90 ‰. All other parameters are chosen in line with Table 1 of our manuscript with the exception of the singular parameters we vary for each analysis. Our analysis in Fig. S5, shows that our main results are resilient to a change in either of the two parameters. We attribute the small differences to a feedback from the intervention model.

Our model simulates the viral mutation in a two-fold process. The stylized RNA mutation gives rise to new virus variants. This RNA mutability is governed by δ. A new variant mutates its individual epidemiological parameters that it inherited from its parent variant. This parameter mutation distance follows a (limited) normal distribution that depends on σ. The expected effect of a lower RNA mutability is a reduced evolutionary complexity. Indeed, Fig. S5 shows this effect. It also shows that reducing the parameter mutation range has a strong impact on the evolutionary dynamics. By setting $\sigma = 0$ we effectively disable the parameter mutation. The result is a strong reduction of the pairwise diversity and all measures of entropy.

The effect of the parameter mutation cannot be attributed to a singular parameter. As shown in Fig. S6 **A** the absence of the mutation of individual parameters exhibits only a minor effect.

The biggest difference can be observed in a combination of the parameters directly affecting the basic reproduction number R_0: β, γ and μ. This, as shown in **C**, is not due to a rapid increase of the basic reproduction number. Rather, a small differentiation in virulence is sufficient, albeit vital, to produce the observed effect on the viral diversification. The simulated mutations cause R_0 to reach a value, shown in **D**, that is within the observed range for the Omicron variant of SARS-CoV-2 (*36*). Fig. S6 Fig. S6 **b** depicts examples of the synthetic phylogeny after four years with and **E** without the parameter mutation. As visible, a lack of the parameter mutation leads to an unrealistic diversification where the ancestral variant remains the most potent pathogen across all recurring infection waves.

The lethality of our simulated disease interacts with the intervention model. In Fig. S7 we explore this relationship. We consider the example scenarios for our three intervention scenarios and compare them to versions with no initial lethality and no cross-protection. As expected, we find that the initial survival chance λ_0 has a strong impact on the results. An initially low lethality tends to reduce the phylogenetic complexity. This can be attributed to a reduction of the intervention prevalence. In **A** showing the example of the scenario category A, however, we find the opposite effect. Here, after four years the complexity is increased. The likely explanation is a larger susceptible population left for the variants that are children of the ancestral strain. This exemplifies the complex dynamics that unfold through the interplay of the epidemiological, social and evolutionary systems.

Due to the parameter evolution, a lack of the initial lethality does not entirely remove the interventions. Contrary to our intuition, in our model λ appears to evolve towards a higher lethality (see Fig. S6) if the standard deviation of mutations is very high. This is likely because the initial value of the ability of hosts to survive the disease is close to its upper bound of 1. Our model is not suited to fully unravel the complexities of pathogens within human hosts. Usually, within hosts a trade-off between contagiousness and host health emerges (*37*). What is more, since there are no small host communities in our model, highly lethal variants may not go extinct as quickly as expected. Nevertheless, our viral variants are subject to selective pressure due to the interventions and the susceptible population size. Our results could point towards a trade-off on a global epidemiological level where the lethality lowers the cross-immunity through differentiation but inhibits the transmission due to the interventions. The induced delay between recovery and susceptibility due to the non-specific immunity may limit the evolutionary impact of the lethality on the susceptible

host population size.

In other words, the non-specific immunity in combination with the lethality dependent interventions may change the landscape of the evolutionary stable strategies such that pathogens benefit from (a small) lethality.

The cross-protection against lethal infection outcomes ϕ shows less impact on our results. Its damping effect on the lethality can be explored in Fig. S7 **B**. By removing the cross-protection entirely, we find an increased complexity after four simulated years. With cross-protection, the population's adaption to a novel pathogen leads to less lethal cases. In turn, the intervention prevalence drops. Removing this dynamic in the scenario category B leads to ongoing interventions and an infection spike after their discontinuation. This drives the example towards the scenario category C, which exhibits increased late stage complexity metrics.

Effects after four years

The intervention discontinuation after two years causes a significant change of the resulting phylogenetic complexity. In scenario category C, the infection peak that follows the end of interventions is especially large. Therefore, we also analyze the sensitivity two years after the end of the non-pharmaceutical interventions. Fig. S8 depicts the same analysis as in Section 3.0.1 but two years after the intervention discontinuation.

The infection wave following an intervention cessation appears to have little effect on the qualitative analysis of our model's sensitivity. The changed epidemiological model parameters remain rather inconsequential to our results. Both mutational parameters continue to drive the resulting complexity. While the entropy and linearity metrics may exhibit latent structural effects of early differences, the pairwise diversity reflects a lasting impact of these parameters after four years. The unweighted tree degree entropy H^* exhibits an elevated value for the scenario without the parameter mutation. This points to diversification events in child variants where the resulting sub-variants remain unfit to compete against the ancestral strain. These events are likely the result of the infection spike after the intervention discontinuation.

Effects in other scenario categories

The previous analysis focused on the scenario category C. In the other categories, the effect of the non-pharmaceutical interventions on the phylogenetic complexity differs significantly. Hence, we extend our analysis to two example scenarios from the categories A and B. We use the same example scenarios as in our main study. For the scenario category B we set the intervention threshold to $\tau_b = 2.5 \cdot 10^{-5}$ and the intervention effect β_b to 90 %. The example of the category A uses an intervention threshold of $\tau_b = 1 \cdot 10^{-6}$ and an intervention effect β_b of 60 %.

Figures S9 and S10 show the effect of various parameters on the non-pharmaceutical intervention phase and thereafter for examples of the scenario categories A and B. Overall, the results remain similar to the previous example of the category C. Again, the effect of the mutation parameters is more pronounced. Especially the category A is characterized by a reduction of interventions. Similarly, the effect of the parameter mutation on the phylogenetic complexity metrics is also reduced, albeit still visible.

In both categories, the effect of the adapted epidemiological parameters becomes more pronounced. This is especially evident in the results after four years. An initial R_0 decrease appears to leave more room for a later differentiation. As the interventions become less prevalent in category B and, especially, A, the minimal cross-immunity parameter θ_0 becomes more important for the epidemiological dynamics. Lowering θ_0 increases the resulting evolutionary complexity. This is expected, since this parameter induces a long-lasting non-specific immunity. The larger recovered population in these categories, thus, reduces the mutational complexity. In contrast, a lower recovered population reduces the impact of the cross-immunity on the dynamics in category C (see figures S5 and S8). This emphasizes the fundamental impact of the non-specific immunity on the pathogenic evolutionary complexity.

Vaccination model analysis

We model vaccinations to gauge the possible effect they could have on the progress of the phylogenetic complexity after the repeal of non-pharmaceutical interventions. Our vaccination model is rather simple. A vaccination adds (cross-)immunity against the ancestral strain and a short-lived non-specific immunity. The scenario shown in our main results is optimistic. In it, all citizens that

have not yet been infected can be vaccinated at a rate of 1% of the population per day.

In Fig. S11 **B** we also cover less successful scenarios with lower vaccination rates. One scenario is aimed at vaccinating 81 % of the population and reaching the theoretical herd immunity for the initial R_0 value of 5.4. By the time the vaccine can be distributed, the R_0 value has shifted due to the parameter mutation. In a pessimistic scenario we analyze the effect of a low vaccination rate set to half of that in the optimistic scenario.

Unsurprisingly, the peak infections are lowest in the most effective vaccination scenario. Effects of the vaccination rate on the phylogenetic complexity are visible. In our model, the pharmaceutical interventions reduce the peak of the non-specific immunity that may follow a repeal of the non-pharmaceutical interventions. As a result, the bottleneck effect is reduced.

Such a bottleneck effect may instead be inducible by distributing the vaccine at a very high rate. However, our optimistic vaccination scenario already uses the highest achieved vaccination rate during Covid-19 (*34*).

Empirical development in SARS-CoV-2 and influenza

As a final step in our investigation, we analyze the empirical development of viral pathogenic evolution before, during and after the Covid-19 pandemic. Our hypothesis is that non-pharmaceutical interventions increase the structural complexity of phylogenetic trees of viral pathogens such as influenza and SARS-CoV-2 due to the fact that the population builds less widespread non-specific immunity. Due to the global nature of the response, the pandemic presents a unique opportunity to study the impact of non-pharmaceutical interventions on pathogenic development.

We study empirical phylogenetic trees from the nextstrain platform (*38*). To stabilize the temporal development, we use the ready made trees based on 12 years of influenza's evolutionary history for HA and NA genes respectively. For SARS-CoV-2 we use all available data, since it is only available for a much shorter period at the time of this writing. We prune the trees to their state up to each month from January 2018 to December 2024. Compared to our synthetic phylogenetic trees, the structure of these empirically observed trees cannot be determined with full certainty. In particular, the early evolution of SARS-CoV-2 can only be inferred. This explains the initial low linearity and higher tree degree entropy we find for its phylogenetic tree in Fig. S12 **A**.

Furthermore, the evolution of SARS-CoV-2 had been affected by non-pharmaceutical interventions almost from the beginning. This is why SARS-CoV-2 represents a poor case to study our hypothesis empirically and why we instead use a simulation approach to investigate this 'what if?' type question.

Since we have no information about the infection numbers for specific variants in these trees, we can only use the unweighted versions of our metrics.

During the pandemic, tree linearity Λ and the tree degree entropy H^* suggest a higher evolutionary complexity in SARS-CoV-2 compared to the influenza samples. This matches reported observations in the literature (*2, 3*). The metrics seem to respond to a seasonal development. This is particularly evident in our linearity metric during the winters of 2020 and 2021. Qualitatively, H^* bears the most resemblance to our simulated vaccination example scenario. This metric also shows the highest correlation to the peak non-specific immunity in our simulation study. The phylogenetic entropy index H_p shows a lower value for SARS-CoV-2 compared to influenza viruses. This is likely due to its comparatively low tree size. In both entropy metrics, the development of SARS-CoV-2 appears to align with the phylogenetic trees of influenza viruses after the pandemic.

The analyzed trees represent a filtered subset of the full evolutionary picture. Thus, a quantitative comparison of synthetic and observed phylogenetic trees is difficult. Nonetheless, our analysis unveils characteristic changes in the pathogenic evolution (see Fig. S12 **B**). We test whether the evolution is significantly different using monthly data on the change in each metric.

Starting in March of 2020, for influenza trees, the development of the phylogenetic entropy index H_p and our linearity metric stagnates. Furthermore, it returns, for almost all lineages that we consider, to its previous trend (or closer to the previous trend). This is an important finding which suggests that this is indeed due to the pandemic. These changes in the trend are significant until the end of 2022. For H3N2, this effect is less prominent. A significant difference for the trend in H_p could only be established until October of 2021. Furthermore, the linearity metric shows no significant differences in post-pandemic development for the NA gene. Contrary to our other findings, the NA gene of the influenza B victoria lineage exhibits an even stronger stagnation in its development after the pandemic. Further research is necessary to explain these differences and to investigate whether they will persist.

We observe a strong effect of the Covid-19 pandemic on the tree degree entropy metric H^*.

From June 2020 until the end of 2022 we observe a significant mean increase of entropy in contrast to a decrease before and thereafter. There are no significant differences between the pre- and post-pandemic development, which again supports our hypothesis that the pandemic is the driving force behind these results.

To conclude, our empirical analysis uses ready made phylogenetic trees that are pruned to specific dates. It shows that the phylogenetic tree structure metrics used in our analysis have a potential to shed light on viral pathogenic evolution. Importantly, we find that the pandemic seems to have affected influenza's evolution, albeit this is likely of a temporary nature. While our empirical analysis is not able to establish a causal link, our simulations point to social distancing as a driver of these changes. Our findings highlight the essential link between social and natural systems and may act as an important stepping stone for further research.

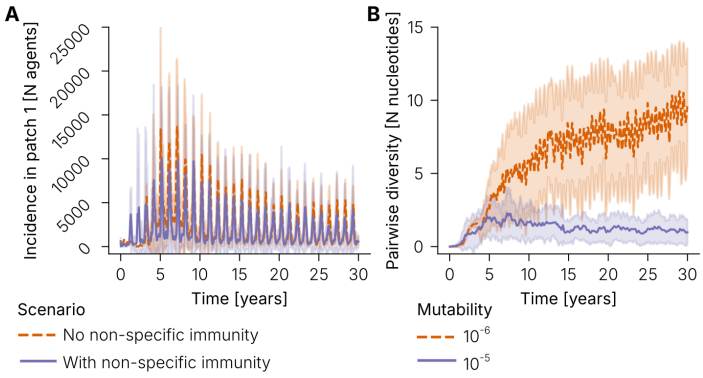

Figure S1: **Reproduction of the influenza reference model's results [see (*1*)] using our model with the assumption of perfect mixing withing geographical patches.** Both panes show the mean and standard deviation of 20 simulation runs comparing a scenario with low mutability but no non-specific immunity component with a scenario using high mutability and a non-specific immunity. (**A**) Incidences observed in the first geographical patch matching the reported numbers closely. (**B**) Pairwise nucleotide diversity weighted by the case abundance. The effect of the non-specific immunity component is evident in the low diversity exhibited despite a higher mutation rate in the scenario with non-specific immunity.

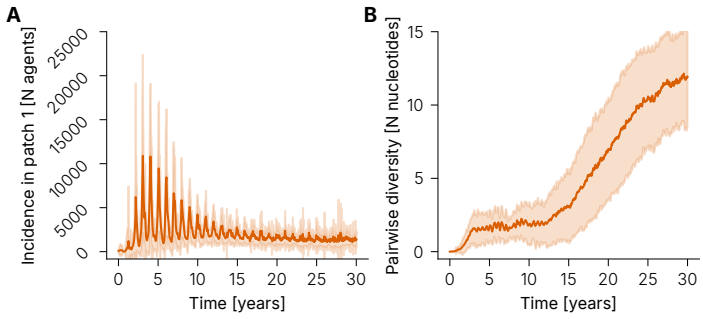

Figure S2: **Starting simulation runs close to the single-strain equilibrium using our adapted model without interventions shows a similar evolution to the influenza reference model [see (*1*)] until approximately year** 15**.** (**A**) The seasonality effects in the first geographical patch's incidence fade over time. (**B**) After some 15 years the effect of the parameter mutation drives our results towards a higher pairwise diversity. As shown in our manuscript, it is vital to assess the impact of the parameter mutation for a novel pathogen. However, our model does not set any limits to the evolution of the epidemiological parameters beyond their defined range. We, therefore, conclude that our long term analysis should focus on the model state after 15 years.

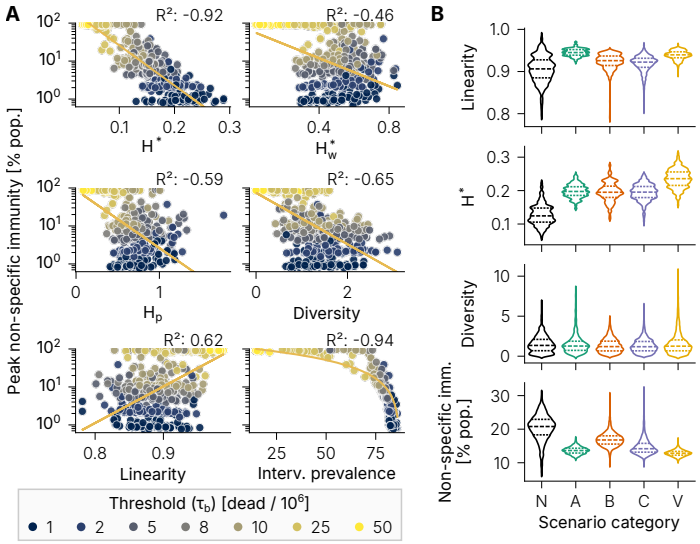

Figure S3: **The same correlation analysis exercised for the intervention effect β_b in our manuscript's main results can be extended to the intervention threshold τ_b.** (**A**) The correlation of most metrics is not as strong for this intervention parameter. Only the pairwise diversity metric gives a stronger response than when varying the intervention effect which was set to 90 % for this graph. (**B**) The state in year 15 of variables that were omitted in our main results for spatial reasons. The long term effects of the interventions seem to increase our linearity metric. The entropy metrics remain elevated. A possible explanation for this phenomenon is the increasing number of diversification events and the comparatively late emergence of differentiation in the scenario without interventions. The pairwise diversity appears to find a similar equilibrium in all scenarios. The population with non-specific immunity is larger in the scenario without interventions. In Fig. S4, we find that this difference reduced after 30 simulated years.

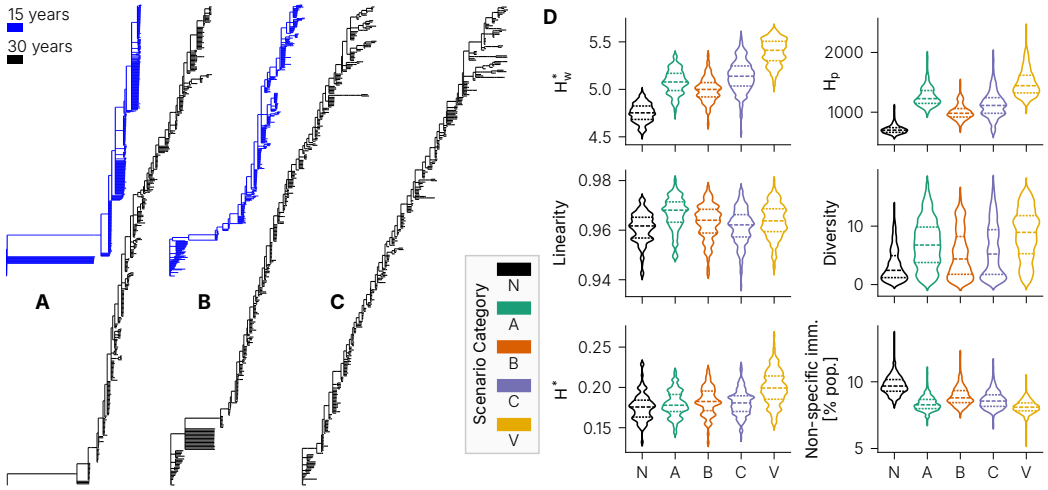

Figure S4: **In the 30th simulated year the complexity remains higher for scenarios with interventions.** There seems to be an increasing effect of the parameter mutation that drives diversity in these scenarios. The scenario without interventions appears to remain more resilient to this effect. (**A**) Example trees after 15 (blue) and 30 (black) years for a scenario without interventions. (**B**) Synthetic phylogenetic trees for the scenario category C after 15 (blue) and 30 (black) years. (**C**) An example tree for a vaccination scenario with 1 % vaccination rate after 30 years. For all phylogenetic trees we only show the 500 variants with the largest recovered population and their ancestors. For the sake of comparison, all trees are generated using the same random number generator seed. The associated metrics for these trees can be found in Table S5. (**D**) The state of our focused metrics after 30 simulated years. The entropy metrics are mostly differentiated through latent effects of early diversification events. Pairwise diversity is driven higher in scenarios with interventions due to the epidemiological parameter mutation.

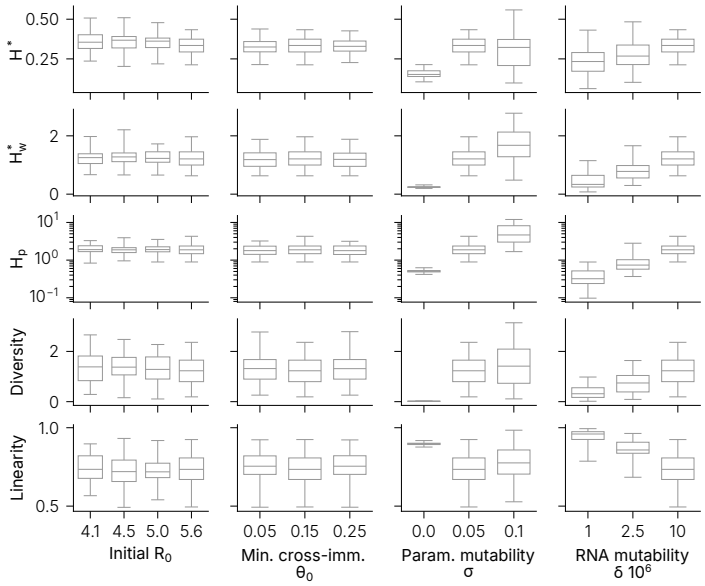

Figure S5: **A sensitivity analysis of the intervention scenario with $\tau_b = 10^{-6}$ and an intervention effect β_b of 90 % shows a large impact of changes in mutational dynamics on our main results.** The effect of the adapted epidemiological parameters is comparatively small. The investigated scenario was chosen as an example of the scenario category C. The R_0 values refer to the transmission within geographical patches. The fourth column shows the three mutability values for the stylized RNA also used by the influenza reference model [see (*1*)]. A lower mutability leads to less variant offspring and, thus, a reduction of the diversity and the opportunity for the epidemiological parameters to diverge. The parameter mutation, shown in the third column, only takes effect in new variants. Effectively disabling the parameter mutations by setting $\sigma = 0.0$ strongly reduces the effect of the interventions on all used metrics.

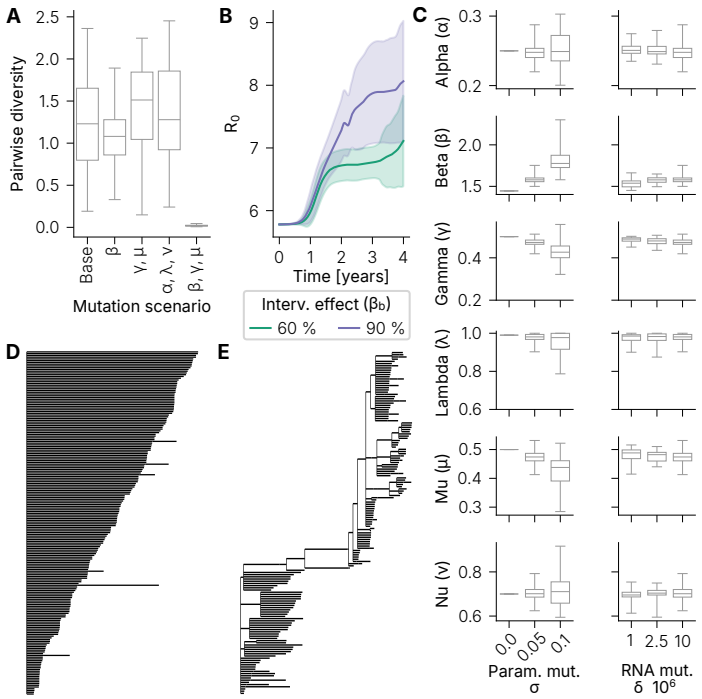

Figure S6: **The consequences of removing the parameter mutation cannot be explained by a drastic impact on one singular parameter.** Removing the mutation of singular parameters does not show the same effect on the pairwise diversity. (**A**) Results of removing the mutation in various combinations of epidemiological parameters. A *Base* scenario allows all the epidemiological parameters to mutate. Only the absence of the mutation in all parameters affecting the basic reproduction number (β, γ and μ) leads to a large drop of the pairwise diversity. (**B**) In the example scenario for the category C, the R_0 values mutate towards the range that could be observed for the Omicron variant of SARS-CoV-2 (*36*). (**C**) Despite the large effect, the amplitude of these mutations is not excessive. A visual comparison of the resulting phylogeny without (**D**) and with (**E**) the parameter mutation underlines its effect and importance. In each tree we show the 200 variants with the most infections and recovered hosts and their ancestors in each tree.

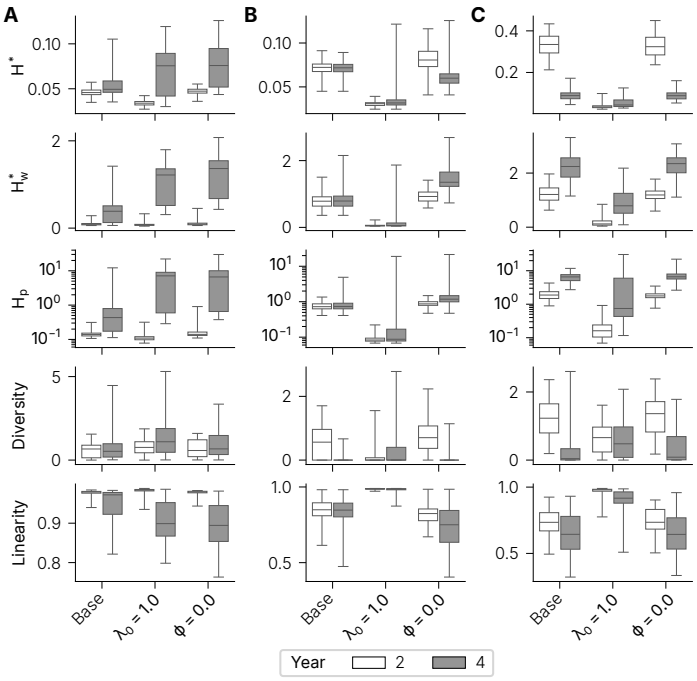

Figure S7: **Raising the initial survival chance λ_0 to 100 % decreases the evolutionary complexity by reducing the intervention prevalence.** (**A**) Result of a scenario without lethality and one without cross-protection for an example of the scenario category A. (**B**) The example scenario for the scenario category B, where the impact of lethality is especially visible. (**C**) An example of the category C, where this effect is also pronounced. In contrast, (**A**) shows that a lowered lethality can increase the pairwise diversity. We attribute this to a smaller impact of the large first infection wave on the susceptible population available to the variants emerging later. Overall the cross-protection ϕ against lethal infection consequences appears to have less impact. In (**B**) its removal slightly increases the observed mutational complexity after four years. This is likely due to the damping effect effect of the cross-protection on the lethality. The lack of this effect leads to prolonged interventions and a larger impact of their discontinuation after two years. The base scenarios refer to the category examples with interventions but unchanged lethality parameters.

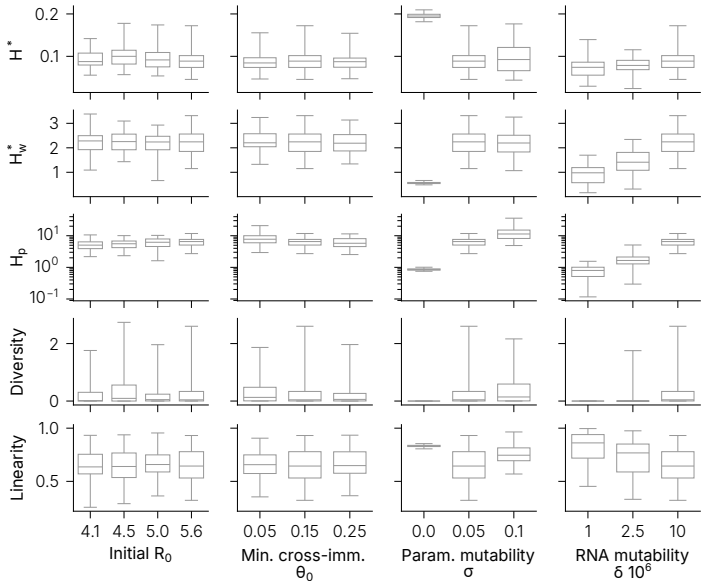

Figure S8: **Two years after the discontinuation of the non-pharmaceutical interventions there is no drastic change in the results of our sensitivity analysis.** The adapted epidemiological parameters continue to show little effect on the main results. In contrast, the mutational parameters still show a strong effect on the results. Lowering the mutation rate, both for the parameter mutation as well as for the stylized RNA mutation, reduces the evolutionary complexity. This effect remains somewhat visible in the pairwise diversity which is less prone to the latent effects of early dynamics. However, the unweighted tree degree entropy H^* shows an increased value for the lowest parameter mutability. This hints at speciation events where child variants spawn offspring still unfit in their competition against the ancestral strain.

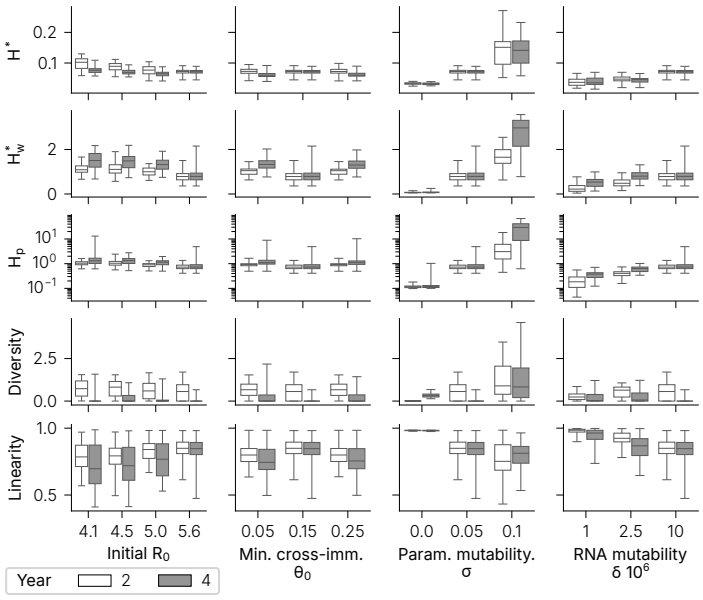

Figure S9: **In the scenario category B the observed effects after** 2 **years of non-pharmaceutical interventions remain mostly unchanged.** A slight reduction of the parameter mutation's effect can be attributed to the lower intervention prevalence. This is also (quantitatively) evident in the results for a higher mutability. Lowering the initial R_0 value seems to leave slightly more room for a later differentiation. A reduced minimal cross-immunity also impacts the long term result. This points to the reduced bottleneck effect of the non-specific immunity component in this scenario.

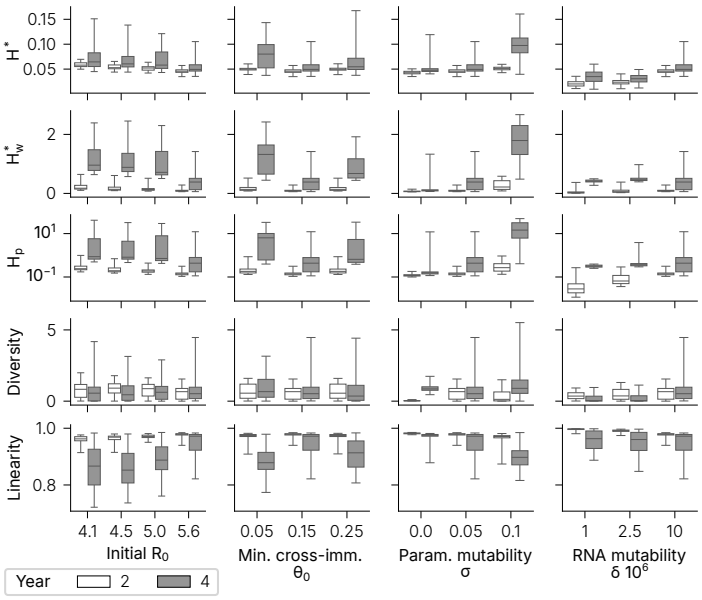

Figure S10: **For the scenario category A we observe a reduced impact of the mutational parameters on the phylogenetic complexity.** This can be attributed to a reduction of the non-pharmaceutical intervention prevalence. The effect still remains visible, pointing to the lasting effect of the initial interventions. The adapted epidemiological parameters show a noticeable effect after the intervention phase. Like in Fig. S9, a reduction of the initial R_0 value may leave more space for a later differentiation. In the category A, the cross-immunity component's effect is even more pronounced. Reducing the minimal cross-immunity parameter θ_0 increases the phylogenetic complexity after four years.

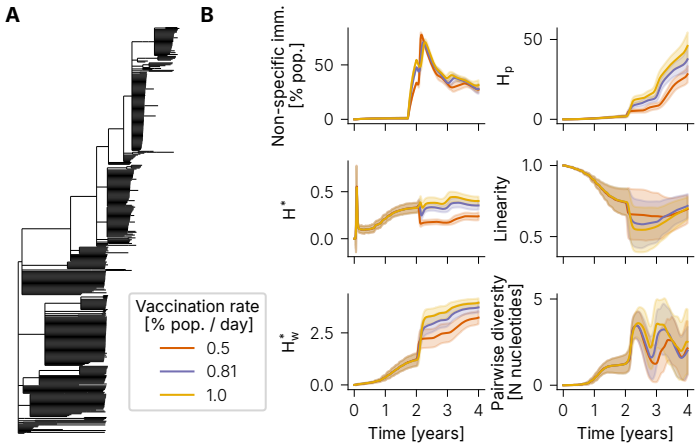

438

439 **Figure S11**: **Different vaccination rates affect the phylogenetic complexity by reducing the**
440 **effective peak size of the non-specific immunity.** (A) An example of a synthetic phylogenetic
441 tree produced by a scenario with the highest vaccination rate. The vaccination mitigates a variant-
442 induced bottleneck effect and, thus, creates an equal playing field for all variants. This increases
443 the evolutionary complexity as it is quantified by our metrics. (B) The temporal development in
444 the first for years in three vaccination scenarios. The reduced bottleneck effect can be traced in
445 all indicators. A lower vaccination rate leads to a higher entropy, a slight increase of the pairwise
446 diversity and a decreased linearity. The vaccination rates were chosen based on three scenarios. In
447 the optimistic scenario, the population is vaccinated at a rate of 1 % per day. Not all citizens can be
448 vaccinated due to some having been infected recently. An additional scenario was chosen where the
449 theoretic herd immunity should be reached at 81 % of vaccinated citizens. Finally, the lowest rate
450 is set to half of the optimistic scenario in an attempt to model an insufficient vaccination progress.

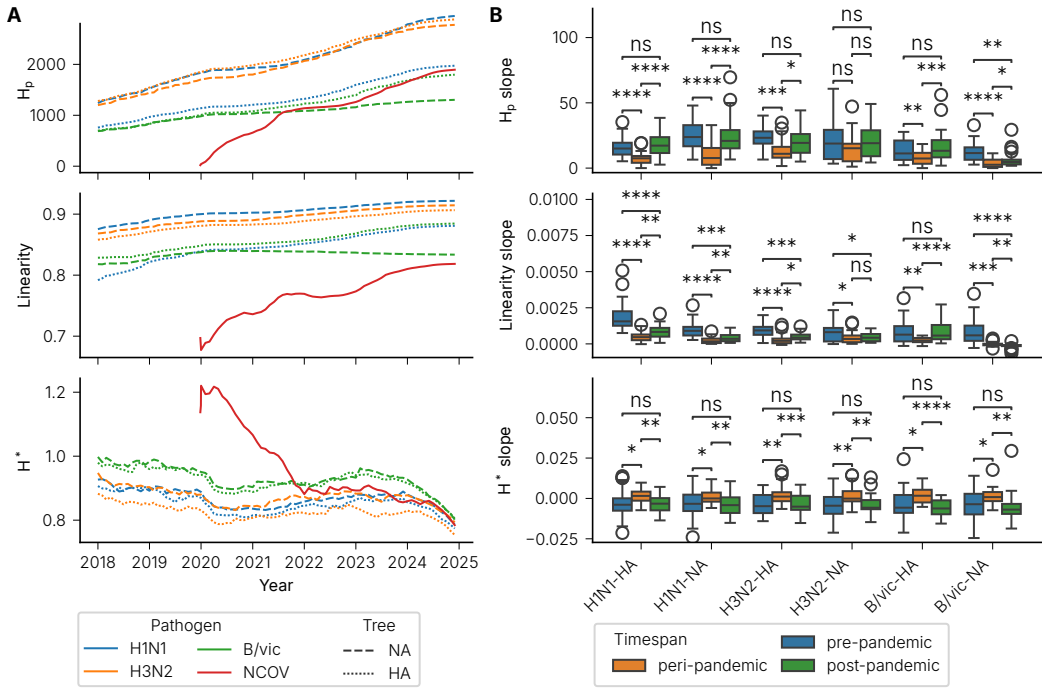

Figure S12: **Observed phylogenetic trees of influenza exhibit characteristic changes in the development of entropy and linearity during the pandemic.** (**A**) Temporal development of our complexity metrics applied to phylogenetic trees of influenza viruses in comparison to SARS-CoV-2 covering pre-pandemic to post-pandemic evolution. Our tree linearity metric Λ can observe the higher complexity of SARS-CoV-2 described in the scientific literature. It also appears to show an effect of the pandemic on the evolution of influenza viruses. Their tree degree entropy H^* exhibits a rapid initial decline with the onset of interventions followed by a subsequent growth that may be the result of reduced non-specific immunity. The tree degree entropy of SARS-CoV-2 peaks during 2020 and starts to align with influenza results after two years. The phylogenetic entropy index H_p of SARS-CoV-2 is lower due to its size. After the pandemic, the development approaches that of influenza. All metrics exhibit seasonal effects with differing prominence. (**B**) The pandemic phase significantly differs from its preceding and following development. However, different temporal selections have to be made. For the phylogenetic entropy index H_p, we find a slowed growth that is likely due to the early, intended effect of interventions following March 2020, most probably due to its correlation with tree size growth (see Table S4). Our linearity metric also exhibits a slowed growth that lasts from March 2020 to the end of 2021. The tree degree entropy H^* shows a significant growth from June 2020 until the end of 2022. This trend follows an initial decrease that is likely caused by the onset of interventions.

Table S1: The parameters used for the simulation study. Some parameters, such as the intervention effect and threshold vary by simulated scenario and are not listed here.

Name	Value	Description	Source
L	30	Agent lifespan.	(*1*)
M	20	Number of geographical patches.	(*1*)
N_p	$\frac{12{,}000{,}000}{M}$	Number of inhabitants per patch p.	(*1*)
α	0.25	Average latent period of 4 days.	(*12*)
$\beta_{W,0}$	$\frac{289}{200}$	Infectiousness within a patch with $R_0 = 5.4$.	(*1, 32*)
h	$\frac{269}{289}$	Infectiousness across patches with $R_0 = 0.02$.	(*1, 32*)
γ_0	0.5	Average 2 days of (a-)symptomatic period.	(*12*)
λ_0	0.99	Chance of survival.	(*12*)
μ_0	0.5	Average 2 days of pre-symptomatic period.	(*12*)
ν_0	0.7	Fraction of symptomatic infections.	(*12*)
ϵ_p	-0.25 / 0.25	Seasonality, negative if patch $p > M/2$.	(*1*)
ψ	0.99	Cross-protection against death.	(*12*)
τ	$\frac{1}{270}$	Decay rate of non-specific immunity.	(*1*)
σ	0.05	Standard deviation of parameter mutation.	(*12*)
δ	10^{-6} - 10^{-5}	Mutation rate of nucleotide bases per infectious host per day.	(*1*)
θ_0	0.15	Minimum cross-immunity effect.	(See Section 3)
θ_1	0.99	Maximum imperfect cross-immunity effect.	(*1*)
n_t	2	Antigenic distance threshold.	(*1*)

Table S2: The parameters used for the reproduction model. All parameters are derived from the influenza reference model [see (*1*)]. The minimal cross-immunity effect θ_0 is adapted to the differences in the the cross-immunity model. The contact rate $\beta_{W,0}$ and the homophily h are derived from the influenza reference model's values as described in Section 3.0.1.

Name	Value	Description
L	30	Agent lifespan.
M	20	Number of geographical patches.
N_p	$\frac{12{,}000{,}000}{M}$	Number of inhabitants per patch p.
α	0.5	Average latent period of 2 days.
$\beta_{W,0}$	$\frac{289}{200}$	Infectiousness within a patch with $R_0 = 5.4$.
h	$\frac{269}{289}$	Infectiousness across patches with $R_0 = 0.02$.
γ_0	0.25	Average 4 days of infected period.
ϵ_p	-0.25 / 0.25	Seasonality, negative if patch $p > M/2$.
τ	$\frac{1}{270}$	Decay rate of non-specific immunity.
δ	10^{-6} - 10^{-5}	Mutation rate of nucleotide bases per infectious host per day.
θ_0	0.15	Minimum cross-immunity effect.
θ_1	0.99	Maximum imperfect cross-immunity effect.
n_t	2	Antigenic distance threshold.

Table S3: Correlation between metrics and the phylogenetic tree size.

	Tree size	PD	Λ	H^*	H^*_w	H_p
Tree size	1.000000	-0.045520	-0.216350	-0.361966	0.326739	0.536647
PD	-0.045520	1.000000	-0.306345	0.343543	0.316502	0.250051
Λ	-0.216350	-0.306345	1.000000	-0.427979	-0.915686	-0.628884
H^*	-0.361966	0.343543	-0.427979	1.000000	0.424715	0.212379
H^*_w	0.326739	0.316502	-0.915686	0.424715	1.000000	0.837813
H_p	0.536647	0.250051	-0.628884	0.212379	0.837813	1.000000

Table S4: Correlation between temporal metrics differences and the phylogenetic tree size differences.

	Δ Tree size	ΔPD	$\Delta\Lambda$	ΔH^*	ΔH^*_w	ΔH_p
Δ Tree size	1.000000	0.394419	-0.725089	0.102415	0.802855	0.894748
ΔPD	0.394419	1.000000	-0.309248	0.051063	0.391713	0.439709
$\Delta\Lambda$	-0.725089	-0.309248	1.000000	-0.098356	-0.934172	-0.780769
ΔH^*	0.102415	0.051063	-0.098356	1.000000	0.115777	0.107378
ΔH^*_w	0.802855	0.391713	-0.934172	0.115777	1.000000	0.916460
ΔH_p	0.894748	0.439709	-0.780769	0.107378	0.916460	1.000000

Table S5: Associated values for complexity metrics of the example trees shown in Fig. S4.

Year	β_b [%]	τ_b	$\delta_v \left[\frac{\%}{\text{day}}\right]$	Scen. Category	Λ	PD	H_p	H^*	H_w^*
15	0	-	-	N	0.89	0.63	25.12	0.10	2.31
15	99	10^{-6}	-	C	0.96	2.07	266.54	0.18	4.30
30	0	-	-	N	0.97	0.32	646.20	0.16	4.60
30	99	10^{-6}	-	C	0.97	2.50	1004.85	0.16	5.13
30	99	10^{-6}	1	V	0.99	7.14	1367.60	0.19	5.35